



Research article

Biochar pyrolyzed from MgAl-layered double hydroxides pre-coated ramie biomass (*Boehmeria nivea* (L.) Gaud.): Characterization and application for crystal violet removal



Xiao-fei Tan ^{a, b}, Yun-guo Liu ^{a, b, *}, Yan-ling Gu ^{a, b}, Shao-bo Liu ^{c, d}, Guang-ming Zeng ^{a, b}, Xiaoxi Cai ^{a, b}, Xin-jiang Hu ^{a, b, e}, Hui Wang ^{a, b}, Si-mian Liu ^{a, b}, Lu-hua Jiang ^{a, b}

^a College of Environmental Science and Engineering, Hunan University, Changsha 410082, PR China

^b Key Laboratory of Environmental Biology and Pollution Control (Hunan University), Ministry of Education, Changsha 410082, PR China

^c School of Metallurgy and Environment, Central South University, Changsha 410083, PR China

^d School of Architecture and Art, Central South University, Changsha 410083, PR China

^e College of Environmental Science and Engineering Research, Central South University of Forestry and Technology, Changsha 410004, PR China

ARTICLE INFO

Article history:

Received 20 January 2016

Received in revised form

19 July 2016

Accepted 5 August 2016

Available online 31 August 2016

Keywords:

Biochar

MgAl-layered double hydroxides

Composite

Ramie (*Boehmeria nivea* (L.) Gaud.)

Crystal violet

ABSTRACT

A novel biochar/MgAl-layered double hydroxides composite (CB-LDH) was prepared for the removal of crystal violet from aqueous solution by pyrolyzing MgAl-LDH pre-coated ramie stem (*Boehmeria nivea* (L.) Gaud.). Pyrolysis played dual role for both converting biomass into biochar and calcining MgAl-LDH during the pyrolysis process. Scanning electron microscopy (SEM), transmission electron microscopy (TEM), energy-dispersive X-ray analysis (EDS), X-ray photoelectron spectroscopy (XPS), Fourier transform infrared (FTIR) and zeta potential analysis were used to characterize the CB-LDH. The results of characterization suggested that the calcined LDH was successfully synthesized and coated on biochar. The resulted CB-LDH had higher total pore volume and more functional groups than the pristine biochar. Adsorption experimental data fitted well with the pseudo-second order kinetics model and the Freundlich isotherm model. The rate-controlled step was controlled by film-diffusion initially and then followed by intra-particle diffusion. Thermodynamic analysis showed that the adsorption of crystal violet was a spontaneous and endothermic process. The higher pH and temperature of the solution enhanced the adsorption performance. CB-LDH could also have excellent ability for the removal of crystal violet from the actual industrial wastewater and groundwater with high ionic strength. LDH adsorption, electrostatic attraction, pore-filling, π - π interaction and hydrogen bond might be the main mechanisms for crystal violet adsorption on CB-LDH. The results of this study indicated that CB-LDH is a sustainable and green adsorbent with high performance for crystal violet contaminated wastewater treatment and groundwater remediation.

© 2016 Elsevier Ltd. All rights reserved.

1. Introduction

Considerable amount of dyes and pigments effluents of industries (such as textiles, printing, plastics, leather and food) are discharged into water (Gessner and Mayer, 2001), which can pose a significant threat to ecosystem. Synthetic dye is one of the most serious contaminants in aquatic environments due to its large-scale production, commercial importance, extensive application, slow biodegradation and toxicity (Forgacs et al., 2004). Their presence in

effluents and industrial wastewaters is of considerable interest because of health risks carried by the potential for contamination of soil, groundwater and drinking water supplies (Carneiro et al., 2010). Many investigations have proved that the synthetic dyes (including azo, anthraquinone, triphenylmethane, heterocyclic and polymeric dyes) are toxic and could seriously contaminate the groundwater (Dubey et al., 2010; Forgacs et al., 2004; Michaelidou et al., 1995; Travis, 1997). As a representative of synthetic dyes, crystal violet can also pollute groundwater. Travis (1997) reported that the groundwater in Basel was polluted by synthetic dye such as crystal violet (aniline violet), which was arising from the activities of dye manufacture industry. Crystal violet (also known as methyl violet, gentian violet, aniline violet or hexamethylparosaniline chloride) is widely used as a pH indicator, as a purple dye for

* Corresponding author. College of Environmental Science and Engineering, Hunan University, Changsha 410082, PR China.

E-mail addresses: hnliuyunguo@gmail.com, liuyunguo@hnu.edu.cn (Y.-g. Liu).

textiles and inks, and as an additive in medicine (Rushing and Bowman, 1980). Many researchers have reported that crystal violet could induce carcinogenic effects in rodents (Docampo and Moreno, 1990; Littlefield et al., 1985). The toxicity of single oral doses of crystal violet was determined to be as follows per kilogram: 1.2 g and 1 g for mice (LD₅₀) and rats (LD₅₀), respectively (Docampo and Moreno, 1990). It is also reported to be highly toxic to mammalian cells, and cause severe irritation for skin, eye and digestive tract (Mittal et al., 2010).

Achieving sustainability of remediation of contaminated land (soil or groundwater) and water is the major challenge for the reuse of land and water (Bardos, 2014; Bardos et al., 2011b, 2016). The sustainable remediation should not only assist in accelerating the remediation of existing contaminated land (remediation of pollution), but also minimize the potential of future land contamination (prevention of pollution) (Hou and Al-Tabbaa, 2014). Firstly, we need to prevent the further new contamination of land, i.e., removal of crystal violet from wastewater. At the same time, some measures must be taken to remediate the contaminated land, i.e., remediation of the polluted groundwater. There are a wide range of technologies and materials, which can be applied to remove dyes from aqueous solutions, such as adsorption, catalytic degradation, biodegradation, and membrane filtration (Ahmed and Gasser, 2012; Lau and Ismail, 2009; Wu et al., 2014). Of which, application of biochar for dyes removal is considered as a sustainable and green technique (Tan et al., 2015), which can be applied for the removal of crystal violet from wastewater and the ex-situ remediation of contaminated groundwater.

Sustainability concerns include the environmental, social, and economic consequences of risk-management activities themselves, and also the opportunities for wider benefit beyond achieving risk-reduction goals alone (Bardos, 2014; Bardos et al., 2011a, 2016; Cundy et al., 2013). Compared with other materials, multiple advantages and benefits of using biochar are existed (Fig. 1). Firstly, biochar is a carbon-rich material produced by pyrolyzing biomass

with little or no oxygen (Tan et al., 2015). Its feedstocks are abundant and low-cost, which mainly obtained from agricultural biomass and solid waste (Lehmann, 2007; Tan et al., 2015). Furthermore, the biochar production is cheap with low energy requirements, which is usually produced at relatively low temperatures (Tan et al., 2015). In addition, the thermochemical treatment of biomass has energy recovery potential, which can generate biofuels and syngas accompanied with biochar production (Lehmann, 2007). Therefore, five complementary goals can be achieved by applying biochar for the removal pollutants from aqueous solutions: wastewater treatment, groundwater remediation, waste management, carbon sequestration, and energy production (Fig. 1) (Tan et al., 2015, 2016).

The removal capacity of biochar for various contaminants depends on its physical and chemical properties, which are greatly affected by the feedstocks, pyrolysis technologies and pyrolysis conditions (Tan et al., 2015). As a result, the raw biochar has limited capacity to adsorb pollutants. So that, a plenty of investigations have also been carried out to produce engineered/modified biochars with novel structures and surface properties by synthesizing biochar based composites (Tan et al., 2016). The adsorption abilities of biochar materials for crystal violet have been studied by many researchers. These studies suggested that the engineered/modified biochar exhibited much better performance than raw biochar. A corncob-based biochar was prepared and applied for crystal violet removal from aqueous solution. The adsorption capacity of this biochar for crystal violet at 25 °C was calculated to be 81.96 mg/g (Fang, 2012). In the further study, a magnetic biochar coated with Fe₃O₄ nanoparticles was synthesized and used for crystal violet adsorption. The adsorption capacity of the magnetic biochar was much higher than the previous raw biochar, which reached to 349.40 mg/g (at initial crystal violet concentration of 400 mg/L, pH of 6.0, and temperature of 40 °C) (Sun et al., 2015).

Layered double hydroxides (LDHs), also known as hydrotalcite-like materials, are homogeneous, basic, and mixed metal hydroxides with

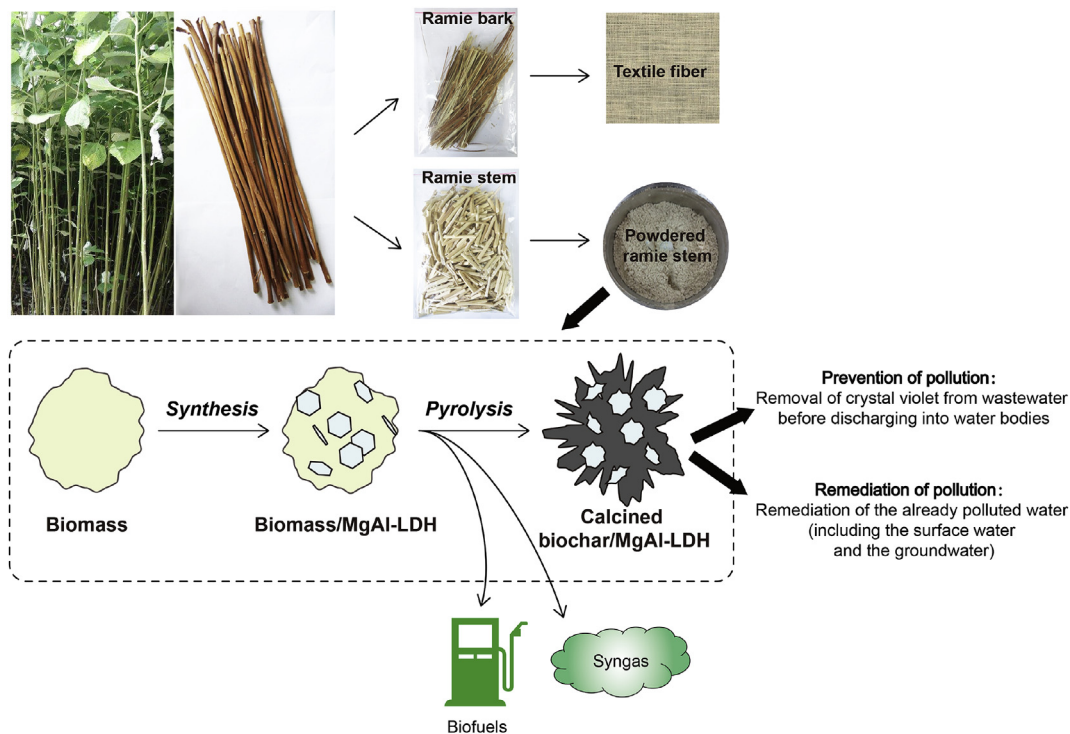


Fig. 1. Illustration of the production process of CB-LDH and its application in wastewater treatment and groundwater remediation.

a lamellar structure (Ahmed and Gasser, 2012; Alvarez-Ayuso and Nugteren, 2005). Their chemical structure can be expressed as the general formula $[M_{1-x}^{2+}M_x^{3+}(OH)_2]^{x+}(A^{n-})_{x/n} \cdot mH_2O$, where M^{2+} and M^{3+} are di- and trivalent metal cations, respectively; A^{n-} is an exchangeable anion; and x is the molar ratio of $M^{3+}/(M^{2+} + M^{3+})$ and the layer charge will depend on the M^{2+}/M^{3+} ratio (Cavani et al., 1991). Calcined LDHs (CLDHs) have the ability to reconstruct their original layered structure after adsorption of various anions, which is so-called “memory effect” (Lv et al., 2006a). LDHs and CLDHs have been widely applied as adsorbents to remove dyes from aqueous solutions in the recent decade (Ai et al., 2011; Shan et al., 2014). Considering the superior properties of LDHs, the application of LDHs to functionalize biochar materials might be a potent method for improving biochar adsorption capacity, so that expand its application in the practical wastewater treatment and groundwater remediation. In addition, biochar can serve as a carrier material for the MgAl-LDH, which helps to minimize the pulverization of hydrotalcite (Zhu et al., 2015). According to the above-explained considerations, the application of MgAl-LDH functionalized biochar can be a potential strategy for improving the sustainability of the remediation of contaminated groundwater (Fig. 1). However, no available research has been conducted to investigate the adsorption of dyes to biochar based CLDH composites.

Ramie (*Boehmeria nivea* (L.) Gaud.) is widely planted in Asian countries such as China, India and Thailand, where its bark has been used for long as a textile fiber (Kipriotis et al., 2015). After bark stripping, the stems which are regarded as agriculture wastes can be recycled as the raw biomass feedstock for biochar production. In the present study, to take advantage of the recent developments in LDHs and biochar, a new biochar based composite (i.e., calcined biochar/MgAl-LDH) was prepared via slow pyrolysis of MgAl-LDH pre-coated ramie stem (Fig. 1). During the pyrolysis process, pyrolysis played dual role for both converting biomass into biochar and calcining nanosized MgAl-LDH simultaneously, which could cut the production cost and time. Furthermore, the characterizations of calcined biochar/MgAl-LDH (CB-LDH) were analyzed. In addition, to estimate the adsorption capacity and understand the mechanism of crystal violet (CV) adsorption onto CB-LDH, the adsorption kinetics, isotherm, and thermodynamics were investigated. For the application of CB-LDH in actual industrial wastewater and groundwater, the effects of pH, background electrolytes and ionic strength on its adsorption capacity for crystal violet were also investigated. The main objective of this study was to develop a feasible method to produce CB-LDH for crystal violet contaminated wastewater treatment and groundwater remediation in a cost-effective way.

2. Methods

2.1. Materials

Ramie used in this study was originally collected from the Ramie Institute of Hunan Agricultural University in China. After the leaves, tops and bark of ramie were removed, the remaining stems were washed with distilled water and dried at 80 °C in a drying oven for 24 h. Then the dried stems were ground to powder and sieved through 2 mm sieve. The powdered ramie stem was stored in airtight plastic containers for later use. All chemicals employed in the experiments were purchased at analytical reagent grade and without any further purification. The molecular structure of crystal violet used in this study is shown in Fig. S1. All the solutions were prepared using high-purity water (18.25 MΩ/cm).

2.2. Preparation of CB-LDH

MgAl-LDH was first synthesized and coated on the biomass feedstock (powdered ramie stem) before pyrolysis (Fig. 1) by a modified liquid-phase deposition method similar to that of Zhang et al. (2013). $AlCl_3 \cdot 6H_2O$ (2.4 g, 0.01 mol) and $MgCl_2 \cdot 6H_2O$ (6.1 g, 0.03 mol) were dissolved in deionized water. 20 g of the ramie stems powder was impregnated with the Mg/Al solution, and then the mixture was shaken at 130 r/min for 24 h. A second solution containing NaOH (16.0 g, 0.4 mol) and Na_2CO_3 (13.25 g, 0.125 mol) in 500 mL deionized water was prepared. The pH was maintained constant by the simultaneous addition of the mixture of Na_2CO_3 and NaOH. The two solutions (Mg/Al solution and the mixture of Na_2CO_3 and NaOH) were added into a three-necked flask, simultaneously and dropwise, while stirring with rotor speed of 500 r/min and maintaining the pH near 10. The resulting slurry was aged at 100 °C for 24 h. The final precipitate was filtered and dried at 80 °C for 36 h to obtain biomass/MgAl LDH. A horizontal tube furnace (SK-1200 °C, Tianjin Zhonghuan Test Electrical Furnace Co., LTD, China) was used to convert these samples into biochar. MgAl LDH-coated biomass powder was filled in a quartz boat and loaded in the quartz tube furnace. Both ends of the quartz tube were sealed and connected with hoses. The chamber of tube furnace was replenished with N_2 (400 mL/min) from one side to keep the inert atmosphere along with the pyrolysis process and the volatile products during biomass pyrolysis are collected from another side. The temperature was programmed to rise up to 500 °C at a rate of 7 °C/min and held at the peak temperature for 2 h before cooling to room temperature. The pristine biochar (PB) without LDH treatment was also produced under the same pyrolysis condition.

2.3. Characterizations

The elemental analyses of all biochars were carried out with an elemental analyzer (Vario EL III, Elementar, Germany). Specific surface areas of adsorbents were measured in a Micromeritics TriStar II 3020 by nitrogen adsorption (77.3 K) and the total pore volume was measured based on the N_2 adsorption-desorption isotherms. The FTIR spectra (Nicolet 5700 Spectrometer, USA) of the adsorbents were recorded in the range of 4000–400 cm^{-1} . The X-ray photoelectron spectroscopy (XPS) measurements were performed using an ESCALAB 250Xi X-ray photoelectron spectrometer (Thermo Fisher, USA). The morphological structure of CB-LDH was characterized by Quanta FEG 250 environmental scanning electron microscopy (SEM) equipped with an energy-dispersive X-ray analyzer (EDS) (AMETER, USA). Electron micrographs of the samples were taken by the transmission electron microscopy (TEM) on FEI Titan G2 60–300 microscope. The zero point charge of CB-LDH was determined using Electroacoustic Spectrometer (ZEN3600 Zetasizer, UK) varying solution pH from 2.0 to 10.0.

2.4. Adsorption experiments

The CV stock solution was prepared to simulate the wastewater and polluted groundwater. The desired concentrations of CV solution were achieved by the dilution of stock solution. The effect of pH on the adsorption of CV was studied at room temperature (299 ± 0.5 K) in 100 mL Erlenmeyer flask containing 0.05 g of adsorbent and 50 mL CV solution. The initial CV solutions (500 mg/L) were adjusted ranging from 2.0 to 10.0 using solutions of NaOH and HCl. The influence of salt ionic strength on the removal of CV (500 mg/L) by CB-LDH was studied with the sodium chloride and calcium chloride concentration varying from 0 to 0.1 M. The removal capacity of CV by PB, LDH and CB-LDH were compared by

mixing 0.05 g of adsorbent with 50 mL CV solution of different concentrations (50, 100, 200, 300, 400, and 500 mg/L). The pH values of the CV solutions were adjusted to 6 and the flasks were shaken for 24 h at room temperature. The samples were then filtered and the CV concentrations were analyzed spectrophotometrically by measuring the absorbance at λ_{\max} 592 nm.

Adsorption kinetics were examined by mixing 0.05 g of adsorbent with 50 mL CV solution (200 mg/L) in 100 mL Erlenmeyer flask at room temperature (299 ± 0.5 K). The pH values of the CV solutions were adjusted to 6. The solutions were shaken at regular intervals, and the adsorbed CV concentrations were determined by the same method after filtration of the solution.

Adsorption isotherm and thermodynamic properties of CV onto CB-LDH was determined by batch sorption experiment under three different temperatures (299, 309, and 319 K) by mixing 0.05 g CB-LDH with 50 mL CV solutions of different concentrations ranging from 50 to 500 mg/L in the 100 mL Erlenmeyer flask. The pH values of the CV solutions were adjusted to 6. The Erlenmeyer flasks were shaken for 24 h. The samples were then withdrawn and filtered to determine adsorbed CV concentrations by the same method.

2.5. Regeneration of used CB-LDH

The regeneration of CB-LDH was conducted by adding CV-loaded CB-LDH to 1 mol/L acetic acid and the mixture was stirred at 299 K and 140 r/min for 2 h. After desorption, the suspension liquid was centrifuged and dried at 353 K for next adsorption experiment. In the adsorption process, the regenerated CB-LDH was added into 50 mL CV solutions of 500 mg/L and shaken at 299 K for 24 h. The samples were then withdrawn and filtered to determine adsorbed CV concentrations.

3. Results and discussion

3.1. Characterization of CB-LDH

The SEM images of CB-LDH are shown in Fig. 2a and b. As can be seen, CB-LDH exhibited irregular surfaces with pores of different shapes and sizes, and the LDHs were deposited on the biochar surfaces evenly. The result of the EDS analysis indicated the existence of magnesium and aluminum on the surface of CB-LDH, which confirmed that the nanosized LDH particles were successfully coated on the biochar surface (Fig. S2c). The TEM image (Fig. 2c and d) revealed that the calcined MgAl-LDH on biochar had collapsed layer structure with no obvious hexagonal dimension, which further indicated that MgAl-LDH was converted to magnesium and aluminum oxides after pyrolysis.

The FTIR spectra of PB and CB-LDH are presented in Fig. S3. The intense band at 3454 cm^{-1} was ascribed to the O–H stretching vibrations of hydrogen-bonded hydroxyl groups. The band at 1631 cm^{-1} was corresponding to C=C stretching vibrations. The intense band at 1443 cm^{-1} was assigned to aliphatic $-\text{CH}_2$ groups. The absorption peaks at 1403 cm^{-1} was assigned to $-\text{COO}-$ symmetric stretching. The band at 1058 cm^{-1} was assigned to the C–O–C stretching vibrations. A series of bands recorded in the $400\text{--}800\text{ cm}^{-1}$ region were ascribed to the M–O and O–M–O (M = Mg, Al) vibration (Goh et al., 2010; Zhang et al., 2013). The FTIR spectra showed that CB-LDH had much higher intensity of the bands of functional groups ($-\text{OH}$, $-\text{COO}^-$, C=C and M–O), which suggested that the introduction of MgAl-LDH significantly increased the proportion of functional groups onto biochar, which may contribute to the higher adsorption capacity of CB-LDH.

To further analysis of the chemical composition on the biochar surface XPS analysis was performed and the results were shown in Fig. 3. The C1s spectrum (Fig. 3a) demonstrated that five

compounds were presented on the CB-LDH surface. The binding energy at 292.64, 289.17, 287.53, 284.71, and 283.89 eV correspond to $-\text{COO}-\text{CH}_2-$, $\text{O}-\text{C}=\text{O}$, $\text{C}=\text{O}$, $\text{C}-\text{C}$ (and $\text{C}=\text{C}$), and $\text{C}-\text{H}$, respectively (Han et al., 2013; Shimada et al., 2007; Solís-Gómez et al., 2014; Steinrück et al., 2006). The existence of $\text{O}=\text{C}-\text{OR}$, $\text{C}-\text{O}$, $\text{C}=\text{O}$, and $\text{O}-\text{H}$ are confirmed by the XPS spectrum of O1s (Fig. 3b) at 535.9, 533.6, 531.2, and 530.62 eV, respectively (Han et al., 2013; Yu et al., 2007; Zhang et al., 2014). These functional groups are consistent with those of FTIR spectra, which can serve as bonding sites for CV. The XPS spectrum of Mg1s and Al2p (Fig. 3c and d) also revealed the formation of MgO (1303.6 eV) (Mittal et al., 2004) and Al_2O_3 (74.14 eV) (Chiu et al., 2005) on biochar surface, respectively. The calcination of MgAl-LDH/biomass resulting in a Mg–Al oxide coated biochar that is capable of being restored to LDH when rehydrated (El Gaini et al., 2009).

3.2. Effect of solution pH on CV adsorption

The solution pH is one of the most vital parameters in the optimization of adsorption process. The effect of pH on the adsorption properties of CV by CB-LDH was determined. As shown in Fig. S4, the removal rate of CV increased with the increase of pH. The initial rapid increase of adsorption may be attributed to the neutralization of the negative charge at the surface of CB-LDH by the positively charged CV molecule (Mittal et al., 2010). The zeta potentials of the CB-LDH are shown in Fig. S4. The pH_{pzc} of CB-LDH was found to be 3.2. Under the solution $\text{pH} < \text{pH}_{\text{pzc}}$, the surface of CB-LDH was positively charged, resulted in the electrostatic repulsion between the positively charged surface and the dye cations. In addition, at lower pH, metal–metal–hydroxysalts may be dissolved and the metal cations in the LDHs layers may be released into solution, which led to the lower CV removal capacity (Lv et al., 2009). CB-LDH carried various surface functional groups (mainly oxygen-containing groups, e.g. $-\text{COOH}$; and $-\text{OH}$). With the increase of pH value, the competition of metal ions and protons for binding sites decreased and more binding sites are released due to the deprotonation of functional groups (Tan et al., 2015). The surface of biochar is negatively charged when $\text{pH} > \text{pH}_{\text{pzc}}$. Therefore, in the higher pH range, the positively charged dye molecules ($=\text{N}^+(\text{CH}_3)_2$) can be easily captured by CB-LDH surface.

3.3. The effect of ionic strength on the adsorption capacity

As the actual industrial wastewater and polluted groundwater usually consist of high concentration of salts, which may affect the CV adsorption. Therefore, the influence of salt ionic strength on the removal of CV by CB-LDH was studied with the sodium chloride and calcium chloride concentration varying from 0 to 0.1 M. The effects of sodium chloride and calcium chloride on the CV adsorption by CB-LDH are shown in Fig. S5. As can be seen, the adsorption capacity for CV changed little with the increase of NaCl concentration. This can be attributed to two evenly matched effects of NaCl: (1) it may restrain the electrostatic interaction between the CV cations and CB-LDH groups and decrease the adsorption capacity with increasing NaCl concentration; (2) on the contrary, it may also enhance the electrostatic interaction between the CV cations and CB-LDH groups by promoting the protonation of CV molecules (Wu et al., 2014). However, CaCl_2 significantly decreased the adsorption capacity and remained almost at the same level with increasing concentration of CaCl_2 (Fig. S5). This may be because that CaCl_2 have much higher screening effect on the electrostatic interaction between the CV cations and CB-LDH groups than NaCl. And, Ca^{2+} may occupy more actives sites, which are available for CV bonding. In the presence of Ca^{2+} , CB-LDH still had the adsorption capacity of 200 mg/g, which suggested that it could have excellent

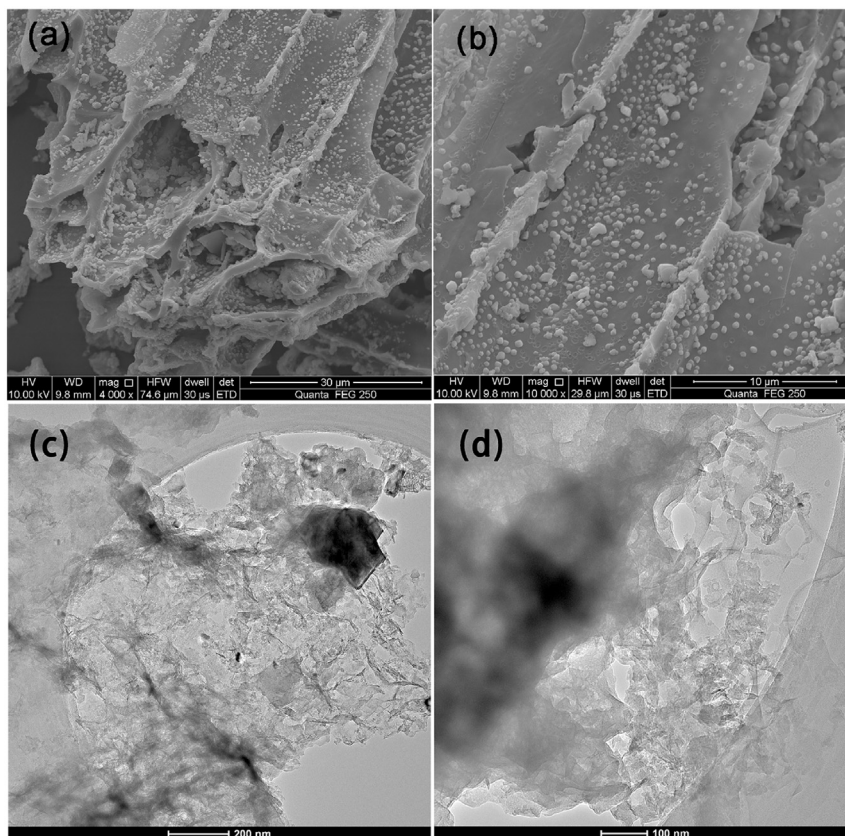


Fig. 2. The SEM images (a, b) and TEM images (c, d) of CB-LDH.

ability for the removal of crystal violet from the actual industrial wastewater and polluted groundwater with high ionic strength.

3.4. Adsorption kinetics

The pseudo-first-order, pseudo-second-order and intra-particle diffusion models were applied to simulate the experimental kinetic data (Hu et al., 2011). Detailed information of those models is described in the Supplementary data. The results of adsorption kinetics studies are shown in Fig. 4a and b and the values of parameters are summarized in Table 1. The data showed a better fit to pseudo-second-order model ($R^2 = 0.987$) than pseudo-first-order model, which can be further confirmed by the excellent accordance between the calculated q_e value and the experimental results. The intra-particle diffusion model was further examined to determine the diffusion mechanisms and identify the possible rate controlling procedure. As shown in Fig. 4c, the plots of q_t against $t^{1/2}$ were multi-linear including three linear portions, indicating that multiple steps were involved in the adsorption process. The values of c_i for all linear sections were not zero (Table S2), which indicated that the intra-particle diffusion participated in the diffusion process but it was not the rate limiting step for the whole reaction (Hu et al., 2011). During the adsorption process, CV molecules were initially adsorbed by the exterior surface of the CB-LDH, that the adsorption of CV onto CB-LDH was firstly controlled by film diffusion. Then, the sorption process was controlled by intra-particle diffusion as CV molecules further entered the pores of CB-LDH and were subsequently adsorbed by the interior surfaces (Ai et al., 2011).

To gain insights into the actual rate-controlling step involved in the overall CV sorption process, the adsorption kinetic data were further analyzed using the Boyd kinetic model (Ai et al., 2011; Boyd

et al., 1947). Based on the analysis of the plot of this model, the actual rate-controlling step (film diffusion or intraparticle diffusion) involved in the overall CV sorption process can be decided. As shown in Fig. 4d, the plot of B_t versus t for the adsorption of CV onto CB-LDH was a straight line and did not pass through the origin, which suggested that film diffusion was the rate-controlling step in the initial adsorption process, and other mechanisms (intra-particle diffusion) took over subsequently.

3.5. Adsorption isotherm

The adsorption equilibrium isotherm was studied using two adsorption isothermal models including Langmuir and Freundlich models (described in the Supplementary data) to fit the experimental data (Fig. 5). The model parameters and the corresponding correlation coefficient (R^2) for the two different models are summarized in Table 1. It can be seen that temperature of 319 K exhibited the highest adsorption capacity for CV. The CV adsorption isotherm data of CB-LDH was fitted better by Langmuir model with the higher correlation coefficient, indicating the adsorption of CV onto the CB-LDH surface was probably a homogeneous and monolayer adsorption process (Sun et al., 2014). Based on the Langmuir model, the maximum adsorption capacity of CB-LDH for CV was 374.686 mg/g at 319 K. In addition, the stability constant (K_1) increased with the increase of temperature, indicating that the bond energy between the surface sites and dye molecules were larger at higher temperature (Sun et al., 2014). The K_1 values in this study were calculated in the range from 0.043 to 0.128 L/mg, indicating that the adsorption between dye molecules and adsorbent was favorable ($0 < K_1 < 1$). These results confirmed the high adsorption capacity of CB-LDH and the pyrolysis of MgAl-LDH

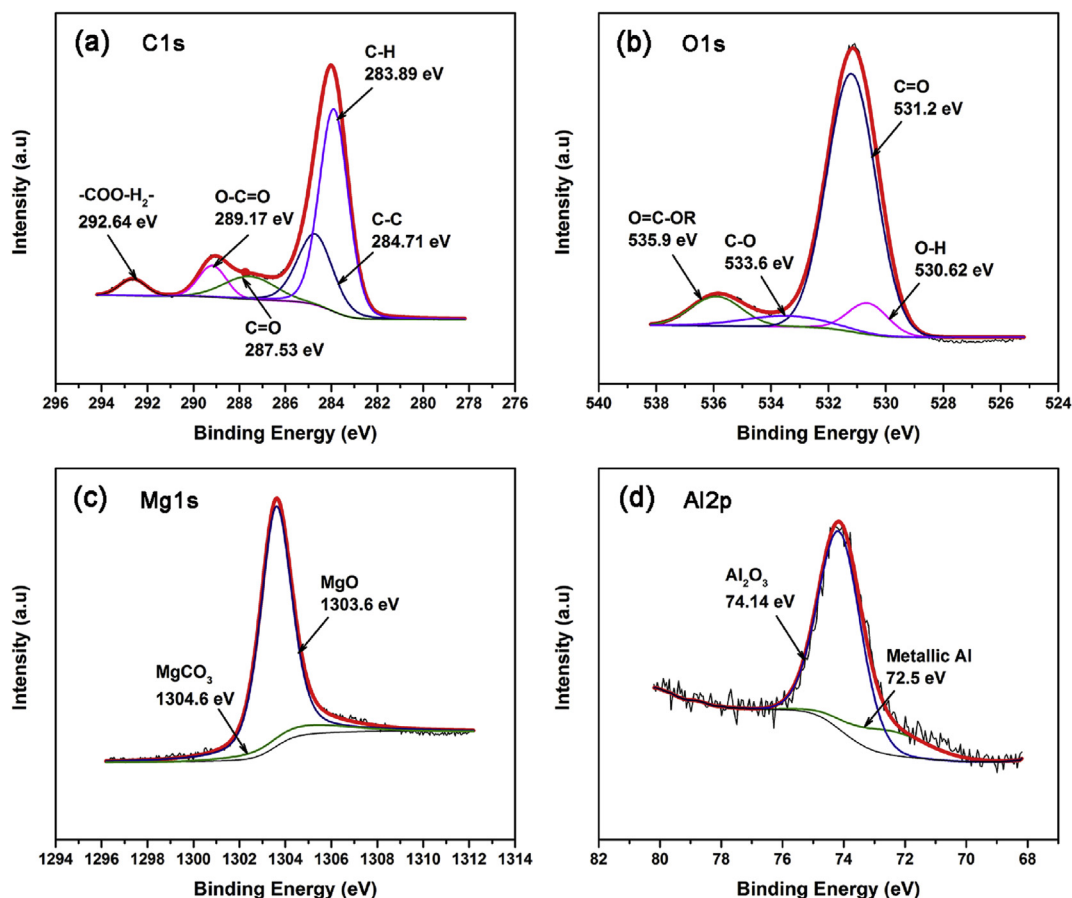


Fig. 3. XPS spectra of CB-LDH: (a) C1s, (b) O1s, (c) Mg1s and (d) Al2p.

pre-coated biomass can be a potent alternative method for the synthesis of biochar based adsorbent.

The comparisons of maximum adsorption capacities of CB-LDH of this study with other adsorbents reported previously for the adsorption of CV are listed in Table S3. As shown in the table, the CV adsorption capacity of CB-LDH is much higher than that of other adsorbents. Such comparison also suggests that CB-LDH may be an effective adsorbent for CV removal from contaminated water.

3.6. Thermodynamic analysis

Thermodynamic analysis was taken to gain further insights into sorption process and mechanisms, and it was investigated at three different temperatures (299, 309 and 319 K). The thermodynamic data, such as Gibbs free energy ΔG^0 , enthalpy ΔH^0 , entropy ΔS^0 , can be calculated using the relevant equations (described in the Supplementary data) (Sun et al., 2014). The linear plot of $\ln K^0$ versus $1/T$ for the adsorption of CV on CB-LDH is shown in Fig. S7. The calculated results are given in Table 2. The negative value of ΔG^0 at three temperatures suggested the feasibility and spontaneous nature of the CV adsorption onto CB-LDH. Furthermore, the ΔG^0 values decreased with the increase of temperature, indicating that the adsorption was more favorable at high temperature. The positive value of ΔH^0 verified the endothermic nature of the adsorption process. The positive value of ΔS^0 might be attributed to the increase of randomness at the solid-solution interface during the adsorption process.

3.7. Regeneration of used CB-LDH

Desorption is another important process reflecting adsorption due to its economical and enhancement value. The results indicated that the adsorption capacity decreased gradually with the increasing of cycles (Fig. S8). After six adsorption/desorption cycles, the adsorbed amount of CV onto the regenerated CB-LDH was 259.32 mg/g, which still remained higher than some reported adsorbents (Table S3). The results indicate that the CB-LDH could be a potential low cost and efficient adsorbent for CV removal due to the excellent regeneration performance.

Table 1

The model parameters and the corresponding correlation coefficient of kinetics and isotherm models.

Kinetics models						
Pseudo-first-order			Pseudo-second-order			
q_e (mg/g)	k_1 (1/min)	R^2	q_e (mg/g)	k_2 (g/mg min)	R^2	
191.705	0.107	0.901	199.294	8.988×10^{-4}	0.987	
Isotherm models						
T (K)	Langmuir			Freundlich		
	q_{max} (mg/g)	K_1 (L/mg)	R^2	K_f (L/mg)	$1/n$	R^2
299	354.050	0.043	0.989	51.633	0.359	0.877
309	364.698	0.075	0.998	72.153	0.320	0.911
319	374.686	0.128	0.975	93.183	0.293	0.932

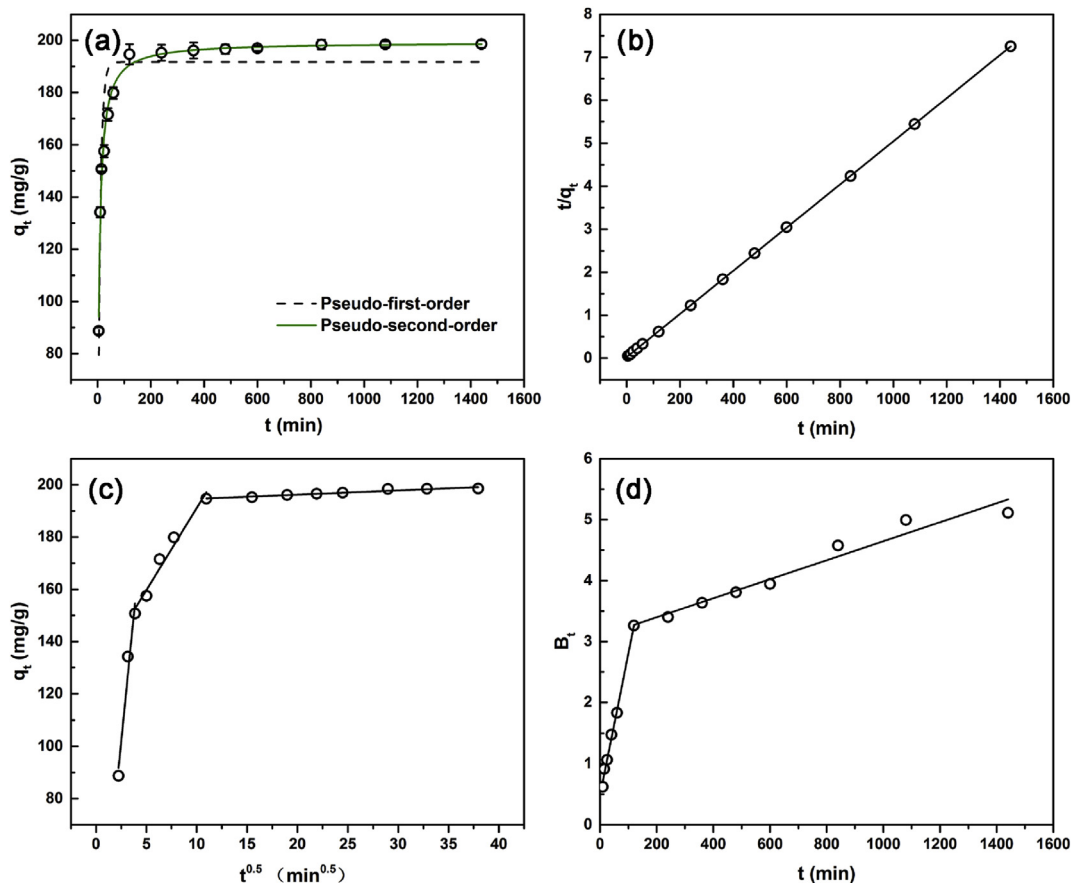
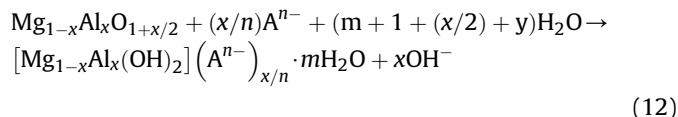
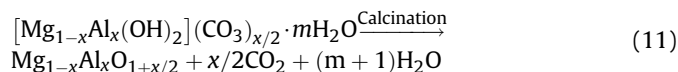


Fig. 4. (a) The kinetics for CV adsorbed by CB-LDH; (b) Modeled result for CV sorption using the pseudo-second-order equation; (c) Intraparticle diffusion plots of adsorption capacity q_t versus the square root of time $t^{0.5}$ for the adsorption of CV onto the CB-LDH; (d) Plots of Boyd parameter B_t versus time t for the adsorption of CV onto the CB-LDH.

3.8. Adsorption mechanisms

By combining the superior characteristic of calcined MgAl-LDH and biochar, CB-LDH can exert multi-effects on the adsorption of CV. Possible mechanisms of the adsorption of CV by the CB-LDH are

proposed in Fig. 6. Calcined MgAl-LDHs have the ability to reconstruct their original layered structure after adsorption (“memory effect”) (El Gaini et al., 2009; Zhu et al., 2005), which can be expressed by the following equations (Lv et al., 2006b):



–Mg–OH, –Al–OH and other groups on the surface of MgAl-LDH after reconstruction could serve as the main adsorption sites for CV cations through the desorption and association of H^+ (Liu et al., 2014). In addition, the deprotonation of various surface functional groups (mainly oxygen-containing groups, e.g. –COOH

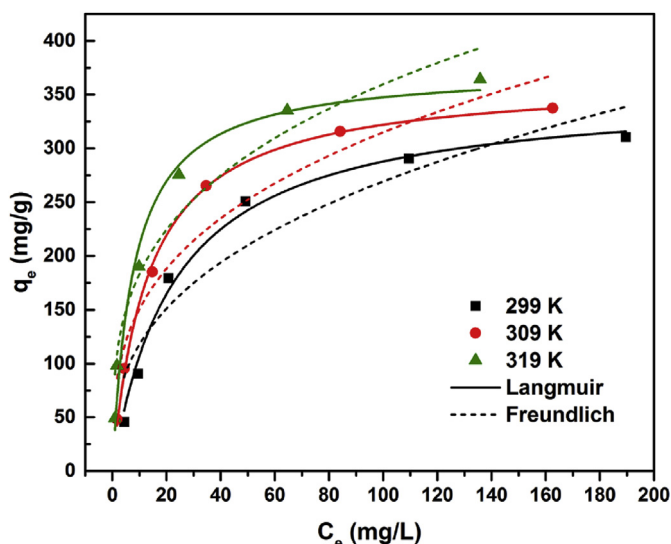


Fig. 5. The equilibrium isotherms for CV adsorbed by CB-LDH at different temperatures.

Table 2
Thermodynamic parameters for CV adsorption on CB-LDH.

Parameters	T (K)		
	299	309	319
$\ln K^{\circ}$	0.833	1.074	1.260
ΔG° (kJ/mol)	–5.697	–7.251	–8.735
ΔH° (kJ/mol)	16.961		
ΔS° (J/mol K)	63.705		

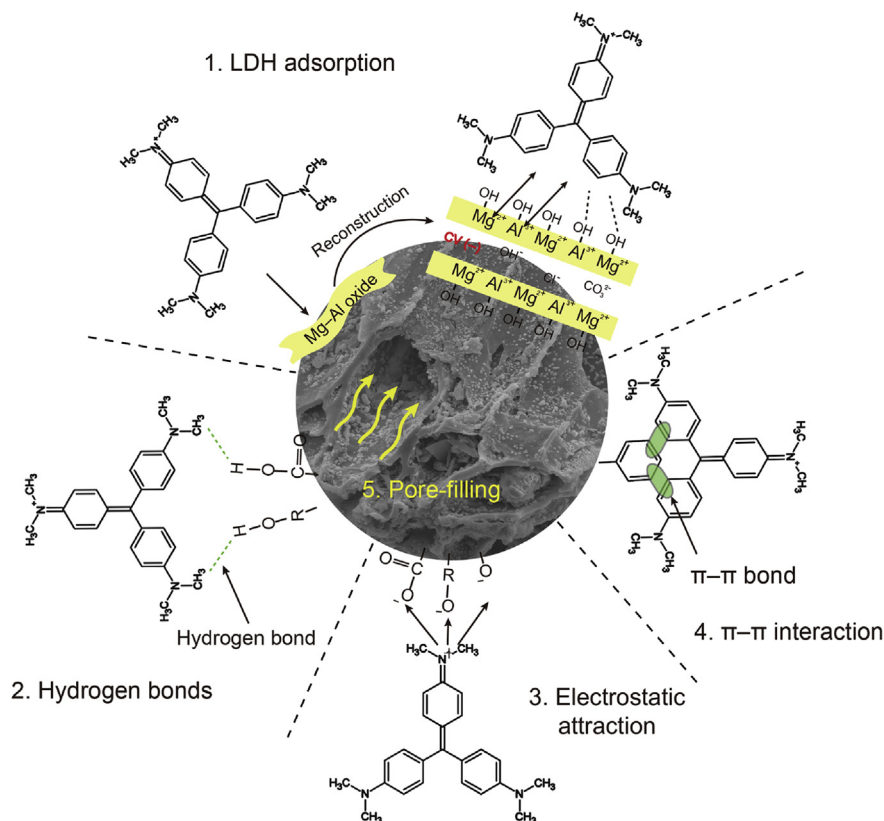


Fig. 6. Adsorption mechanism of CV by CB-LDH.

and $-OH$) may make the surface of CB-LDH negatively charged, which contribute to the electrostatic attraction between CB-LDH and CV cations. In the reconstruction process, anions are intercalated into the layered structure and OH^- ions are released simultaneously. So that, the final pH of the aqueous solution will be increased (Zhu et al., 2005), which can also promote the function of electrostatic attraction. The initial CV solution pH and final pH of the adsorption experiments are listed in Table S4. As can be seen, the final pH significantly increased to near 8.8. At this pH, part of CV can dissociate to CV anion ($pK_a = 8.64$) (Fig. S9), and some can be intercalated into the interlayer space in the reconstructed LDH (Chen et al., 2009). Furthermore, CB-LDH exhibited much higher total pore volume than PB, which may make the CV molecule easier access to the interior surfaces of biochar. This mechanism can also be demonstrated by the analysis of intra-particle diffusion and Boyd kinetic model, which suggested that the intra-particle diffusion controlled the adsorption in the later process. Apart from the mechanisms discussed above, other mechanisms such as $\pi-\pi$ interaction and hydrogen bond, could also be involved in CV adsorption (Wu et al., 2014).

4. Conclusions

The novel biochar based composite was successfully synthesized using ramie stem as the raw biomass feedstock and the calcined MgAl-LDH as the objective functional material. Multiple advantages and benefits of using biochar as the remediation material are existed, including its abundant and low-cost feedstocks (agricultural biomass and solid waste), lower energy requirements during production, carbon sequestration, and concomitant energy production (biofuels and syngas). The results of this study suggested that CB-LDH can be used as an effective, sustainable and

green adsorbent with high performance for crystal violet contaminated wastewater treatment and groundwater remediation, which can fulfill the aim of sustainable remediation of contaminated land (soil or groundwater) by both remediation of pollution and prevention of pollution. Further studies about the synthesis of CB-LDH using other LDHs and biomass feedstock, and their adsorption capacity for other contaminants from wastewater and groundwater should be conducted.

Acknowledgments

The authors would like to thank financial support from the National Natural Science Foundation of China (Grant No. 41271332 and 51521006), and the Hunan Provincial Innovation Foundation for Postgraduate (Grant No. CX2015B090 and CX2015B092).

Appendix A. Supplementary data

Supplementary data related to this article can be found at <http://dx.doi.org/10.1016/j.jenvman.2016.08.070>.

References

- Ahmed, I.M., Gasser, M.S., 2012. Adsorption study of anionic reactive dye from aqueous solution to Mg-Fe- CO_3 layered double hydroxide (LDH). *Appl. Surf. Sci.* 259, 650–656.
- Ai, L., Zhang, C., Meng, L., 2011. Adsorption of methyl orange from aqueous solution on hydrothermal synthesized Mg-Al layered double hydroxide. *J. Chem. Eng. Data* 56, 4217–4225.
- Alvarez-Ayuso, E., Nugteren, H., 2005. Purification of chromium (VI) finishing wastewaters using calcined and uncalcined Mg-Al- CO_3 -hydrotalcite. *Water Res.* 39, 2535–2542.
- Bardos, P., 2014. Progress in sustainable remediation. *Remediation* 25, 23–32.
- Bardos, P., Bone, B., Boyle, R., Ellis, D., Evans, F., Harries, N.D., Smith, J.W., 2011a. Applying sustainable development principles to contaminated land management

- using the SuRF-UK framework. *Remediation* 21, 77–100.
- Bardos, R.P., Bakker, L.M., Slenders, H.L., Nathanail, C.P., 2011b. Sustainability and Remediation, Dealing with Contaminated Sites. Springer, pp. 889–948.
- Bardos, R.P., Bone, B.D., Boyle, R., Evans, F., Harries, N.D., Howard, T., Smith, J.W.N., 2016. The rationale for simple approaches for sustainability assessment and management in contaminated land practice. *Sci. Total Environ.* 563–564, 755–768.
- Boyd, G., Adamson, A., Myers Jr., L., 1947. The exchange adsorption of ions from aqueous solutions by organic zeolites. II. Kinetics. *JACS* 69, 2836–2848.
- Carneiro, P.A., Umbuzeiro, G.A., Oliveira, D.P., Zanoni, M.V.B., 2010. Assessment of water contamination caused by a mutagenic textile effluent/dyehouse effluent bearing disperse dyes. *J. Hazard. Mater.* 174, 694–699.
- Cavani, F., Trifirò, F., Vaccari, A., 1991. Hydrotalcite-type anionic clays: preparation, properties and applications. *Catal. Today* 11, 173–301.
- Chen, S., Xu, Z.P., Zhang, Q., Lu, G.M., Hao, Z.P., Liu, S., 2009. Studies on adsorption of phenol and 4-nitrophenol on MgAl-mixed oxide derived from MgAl-layered double hydroxide. *Sep. Purif. Technol.* 67, 194–200.
- Chiu, L.H., Chen, C.C., Yang, C.F., 2005. Improvement of corrosion properties in an aluminum-sprayed AZ31 magnesium alloy by a post-hot pressing and anodizing treatment. *Surf. Coat. Technol.* 191, 181–187.
- Cundy, A., Bardos, R., Church, A., Puschenreiter, M., Friesl-Hanl, W., Müller, I., Neu, S., Mench, M., Witters, N., Vangronsveld, J., 2013. Developing principles of sustainability and stakeholder engagement for “gentle” remediation approaches: the European context. *J. Environ. Manage.* 129, 283–291.
- Docampo, R., Moreno, S.N., 1990. The metabolism and mode of action of gentian violet. *Drug Metab. Rev.* 22, 161–178.
- Dubey, S., Yadav, R., Chaturvedi, R., Yadav, R., Sharma, V., Minhas, P., 2010. Contamination of Ground Water as a consequence of land disposal of dye waste mixed sewage effluents: a case study of Panipat District of Haryana, India. *Bull. Environ. Contam. Toxicol.* 85, 295–300.
- El Gaiini, L., Lakraimi, M., Sebbar, E., Meghea, A., Bakasse, M., 2009. Removal of indigo carmine dye from water to Mg-Al-CO₃-calcined layered double hydroxides. *J. Hazard. Mater.* 161, 627–632.
- Fang, R., 2012. Preparation of corncob-based bio-char and its application in removing basic dyes from aqueous solution. *Adv. Mater. Res.* 550, 2420–2423.
- Forgacs, E., Cserhati, T., Oros, G., 2004. Removal of synthetic dyes from wastewaters: a review. *Environ. Int.* 30, 953–971.
- Gessner, T., Mayer, U., 2001. Ullmann's Encyclopedia of Industrial Chemistry. Part A27. Triarylmethane and Diarylmethane Dyes. Wiley-VCH, New York.
- Goh, K.H., Lim, T.T., Banas, A., Dong, Z., 2010. Sorption characteristics and mechanisms of oxyanions and oxyhalides having different molecular properties on Mg/Al layered double hydroxide nanoparticles. *J. Hazard. Mater.* 179, 818–827.
- Han, H.S., You, J.M., Jeong, H., Jeon, S., 2013. Synthesis of graphene oxide grafted poly (lactic acid) with palladium nanoparticles and its application to serotonin sensing. *Appl. Surf. Sci.* 284, 438–445.
- Hou, D., Al-Tabbaa, A., 2014. Sustainability: a new imperative in contaminated land remediation. *Environ. Sci. Policy* 39, 25–34.
- Hu, X.J., Wang, J.S., Liu, Y.G., Li, X., Zeng, G.M., Bao, Z.L., Zeng, X.X., Chen, A.W., Long, F., 2011. Adsorption of chromium (VI) by ethylenediamine-modified cross-linked magnetic chitosan resin: isotherms, kinetics and thermodynamics. *J. Hazard. Mater.* 185, 306–314.
- Kipriotis, E., Heping, X., Vafeiadakis, T., Kiprioti, M., Alexopoulou, E., 2015. Ramie and kenaf as feed crops. *Ind. Crop. Prod.* 68, 126–130.
- Lau, W.J., Ismail, A.F., 2009. Polymeric nanofiltration membranes for textile dye wastewater treatment: preparation, performance evaluation, transport modelling, and fouling control—a review. *Desalination* 245, 321–348.
- Lehmann, J., 2007. A handful of carbon. *Nature* 447, 143–144.
- Littlefield, N.A., Blackwell, B.N., Hewitt, C.C., Gaylor, D.W., 1985. Chronic toxicity and carcinogenicity studies of gentian violet in mice. *Fundam. Appl. Toxicol.* 5, 902–912.
- Liu, J., Li, X., Luo, J., Duan, C., Hu, H., Qian, G., 2014. Enhanced decolorisation of methylene blue by LDH-bacteria aggregates with bioregeneration. *Chem. Eng. J.* 242, 187–194.
- Lv, L., He, J., Wei, M., Evans, D., Duan, X., 2006a. Factors influencing the removal of fluoride from aqueous solution by calcined Mg–Al–CO₃ layered double hydroxides. *J. Hazard. Mater.* 133, 119–128.
- Lv, L., He, J., Wei, M., Evans, D.G., Duan, X., 2006b. Uptake of chloride ion from aqueous solution by calcined layered double hydroxides: equilibrium and kinetic studies. *Water Res.* 40, 735–743.
- Lv, L., Sun, P., Gu, Z., Du, H., Pang, X., Tao, X., Xu, R., Xu, L., 2009. Removal of chloride ion from aqueous solution by ZnAl-NO₃ layered double hydroxides as anion-exchanger. *J. Hazard. Mater.* 161, 1444–1449.
- Michaelidou, S.C., Akkeldou, D., Ziegler, P., 1995. Environmental toxicology: hazards to the environment and man in the Mediterranean Region Investigating groundwater pollution from different sources with combined biological and chemical methods. *Sci. Total Environ.* 171, 51–59.
- Mittal, A., Mittal, J., Malviya, A., Kaur, D., Gupta, V., 2010. Adsorption of hazardous dye crystal violet from wastewater by waste materials. *J. Colloid Interface Sci.* 343, 463–473.
- Mittal, V., Bera, S., Nithya, R., Srinivasan, M., Velmurugan, S., Narasimhan, S., 2004. Solid state synthesis of Mg–Ni ferrite and characterization by XRD and XPS. *J. Nucl. Mater.* 335, 302–310.
- Rushing, L.G., Bowman, M.C., 1980. Determination of gentian violet in animal feed, human urine, and wastewater by high pressure liquid chromatography. *J. Chromatogr. Sci.* 18, 224–232.
- Shan, R.R., Yan, L.G., Yang, K., Yu, S.J., Hao, Y.F., Yu, H.Q., Du, B., 2014. Magnetic Fe₃O₄/MgAl-LDH composite for effective removal of three red dyes from aqueous solution. *Chem. Eng. J.* 252, 38–46.
- Shimada, S., Hiroi, T., Ida, T., Mizuno, M., Endo, K., Kurmaev, E.Z., Moewes, A., 2007. X-ray photoelectron and carbon K α emission measurements and calculations of O-, CO-, N-, and S-containing substances. *J. Polym. Sci. Part B Polym. Phys.* 45, 162–172.
- Solis-Gómez, A., Neira-Velázquez, M.G., Morales, J., Sánchez-Castillo, M.A., Pérez, E., 2014. Improving stability of TiO₂ particles in water by RF-plasma polymerization of poly(acrylic acid) on the particle surface. *Colloids Surf. Physicochem. Eng. Asp.* 451, 66–74.
- Steinrück, H.P., Fuhrmann, T., Papp, C., Tränkenschuh, B., Denecke, R., 2006. A detailed analysis of vibrational excitations in x-ray photoelectron spectra of adsorbed small hydrocarbons. *J. Chem. Phys.* 125, 204706.
- Sun, P., Hui, C., Azim Khan, R., Du, J., Zhang, Q., Zhao, Y.H., 2015. Efficient removal of crystal violet using Fe₃O₄-coated biochar: the role of the Fe₃O₄ nanoparticles and modeling study their adsorption behavior. *Sci. Rep.* 5, 12638.
- Sun, Z., Liu, Y., Huang, Y., Tan, X., Zeng, G., Hu, X., Yang, Z., 2014. Fast adsorption of Cd²⁺ and Pb²⁺ by EGTA dianhydride (EGTAD) modified ramie fiber. *J. Colloid Interface Sci.* 434, 152–158.
- Tan, X.F., Liu, Y.G., Gu, Y.L., Xu, Y., Zeng, G.M., Hu, X.J., Liu, S.B., Wang, X., Liu, S.M., Li, J., 2016. Biochar-based nano-composites for the decontamination of wastewater: a review. *Bioresour. Technol.* 212, 318–333.
- Tan, X., Liu, Y., Zeng, G., Wang, X., Hu, X., Gu, Y., Yang, Z., 2015. Application of biochar for the removal of pollutants from aqueous solutions. *Chemosphere* 125, 70–85.
- Travis, A.S., 1997. Poisoned groundwater and contaminated soil: the tribulations and trial of the first major manufacturer of aniline dyes in Basel. *Environ. Hist. Durh. N. C.* 2, 343–365.
- Wu, Z., Zhong, H., Yuan, X., Wang, H., Wang, L., Chen, X., Zeng, G., Wu, Y., 2014. Adsorptive removal of methylene blue by rhamnolipid-functionalized graphene oxide from wastewater. *Water Res.* 67, 330–344.
- Yu, J., Tong, M., Sun, X., Li, B., 2007. A simple method to prepare poly(amic acid)-modified biomass for enhancement of lead and cadmium adsorption. *Biochem. Eng. J.* 33, 126–133.
- Zhang, M., Gao, B., Yao, Y., Inyang, M., 2013. Phosphate removal ability of biochar/MgAl-LDH ultra-fine composites prepared by liquid-phase deposition. *Chemosphere* 92, 1042–1047.
- Zhang, Y.J., Xing, Z.J., Duan, Z.K., Li, M., Wang, Y., 2014. Effects of steam activation on the pore structure and surface chemistry of activated carbon derived from bamboo waste. *Appl. Surf. Sci.* 315, 279–286.
- Zhu, M.X., Li, Y.P., Xie, M., Xin, H.Z., 2005. Sorption of an anionic dye by uncalcined and calcined layered double hydroxides: a case study. *J. Hazard. Mater.* 120, 163–171.
- Zhu, X., Wang, Q., Shi, Y., Cai, N., 2015. Layered double oxide/activated carbon-based composite adsorbent for elevated temperature H₂/CO₂ separation. *Int. J. Hydrogen Energy* 40, 9244–9253.